SEMARAK ILMU PUBLISHING

Journal of Advanced Research in Fluid Mechanics and Thermal Sciences

Journal homepage:
https://semarakilmu.com.my/journals/index.php/fluid_mechanics_thermal_sciences/index
ISSN: 2289-7879

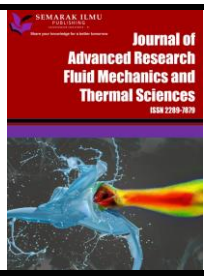

FEM Modelling of the Heating Behaviour in Vibrothermography Based on Thermoelastic Damping on Crack Location

Choosak Ngaongam[1,*], Rapee Ujjin[1]

[1] Department of Aviation Maintenance Engineering, College of Engineering, Rangsit University, Pathum Thani 12000, Thailand

ARTICLE INFO

Article history:
Received 10 May 2023
Received in revised form 5 July 2023
Accepted 11 July 2023
Available online 25 July 2023

Keywords:
Thermoelastic damping; vibrothermography; surface crack; Non-destructive testing (NDT); aircraft material; vibrational frequency

ABSTRACT

The paper aims to simulate the heat generation in crack location based on vibrothermography inspection. For this study, the thermoelastic damping effect was considered as the source of heat generation and the value of thermoelastic damping was determined. In simulation, the model of the specimen with crack was AL7075-T6. The vibrational frequencies were given at 20kHz, 24kHz and 28kHz, while the maximum amplitude was constant of 4.8nm. The results of temperature variation, stress, energy loss and heat flow rate on the crack location were obtained from the simulations which were performed by using ANSYS software. The ratio between power loss and heat flow rate was calculated and presented as the index for selecting the most suitable vibrational frequency in term of heat accumulation. The case study 20kHz was considered as the most suitable vibrational frequency for this study because the index ratio was higher than the case studies 24kHz, 28kHz at 6.29% and 9.14% respectively.

1. Introduction

Vibrothermography inspection is classified as a non-destructive testing (NDT) method. For this technique, the specimen is vibrated and some of the mechanical energy dissipates as heat. Then, the temperature difference between defect and non-defect locations is monitored by using the thermal imaging camera. Vibrothermography inspection has been successfully implemented to inspect for both metallic and non-metallic materials such as titanium, inconel, aluminum alloy, steel, honeycomb structure and carbon fiber reinforced composite (CFRP) [1-8]. All of these materials are widely used to fabricate the aircraft structure. Due to lack of understanding the mechanism of heat generation in vibrothermography, the experiments were performed to investigate the generated heat from the effect of friction, plastic deformation and viscoelasticity [9]. The finite element methods (FEM) were developed to study the frictional effect [10-12]. It found that the friction produced heat along the rubbing surface. The amount of the generated heat depended on the vibrational frequency, surface roughness and the orientation between vibrational direction and defect direction. When the specimen is loaded and the occurred stress is higher than the yield stress of the material. The

* *Corresponding author.*
E-mail address: choosak.n@rsu.ac.th

https://doi.org/10.37934/arfmts.108.1.6674

deformation of specimen is in the plastic range and some of the mechanical energy is converted into heat. However, the generated heat from this case cannot be classified as NDT because it tends to increase the defect size and causes the permanent deformation of the specimen. The effect of plasticity was studied through FEM [13,14]. The heating mechanism of viscoelastic effect was investigated by applying the polymer adhesive over the surface of the vibrating specimen. The mount of the heat depended directly to the strain distribution over the specimen surface [15-17]. The additional mechanism of the heat generation in metallic material is known as thermoelastic damping [18]. The principle of this heating mechanism relates to the stress distribution on the vibrating specimen which usually is non-uniform due to defect. The specimen with defect always has the stress concentration around weakness point at defect location. The generated heat of this mechanism can indicate the defect location without increasing the defect size. Therefore, the effect of thermoelastic damping is considered as the main source of heat generation for this paper. Finite element method (FEM) is developed to simulate the heat generation based on thermoelastic damping. The characteristics of temperature distribution, stress variation, power loss and heat flow rate are analyzed through the results of FEM. Then the suitable vibrational frequency for vibrothermography is analyzed by considering the ratio between power loss and heat flow rate.

2. Numerical Simulation

2.1 Thermoelastic Damping Analysis

The thermoelastic damping (Q^{-1}) can be described as the ratio between the energy loss (ΔW) to the stored energy (W) in one vibrational cycle [19-21]. The mechanical energy loss from this effect converts to heat. While the stored energy of vibrating specimen can be defined as the strain energy which is the input mechanical energy. By multiplying the thermoelastic damping with the strain energy, the energy loss as heat can be calculated. For the thermoelastic damping of the homogenous material can be determined by using Eq. (1) and Eq. (2).

$$(Q^{-1}) = \frac{\alpha^2 E_U T}{\rho C_P} \frac{\omega \tau}{1+(\omega \tau)^2} \tag{1}$$

$$\tau = \frac{h^2}{\pi^2 \chi} = \frac{h^2}{\pi^2 \lambda \rho C_P} \tag{2}$$

where (α) is the linear thermal expansion coefficient, (E_U) is the unrelaxed young' modulus, (ρ) is the density, (C_p) is the specific heat capacity at constant pressure, (τ) is the thermal relaxation time, (λ) is the thermal conductivity and (h) is the thickness of the specimen.

In this study, the material was AL7075-T6 which was used to fabricate the aircraft structure [22-24]. The material properties for calculation the thermoelastic damping calculation were presented in Table 1. In this case study, the specimen thickness 2 mm was given as the remained thickness at crack location. The vibrational frequencies of vibrothermography inspection usually are in the ultrasonic range which are the resonance frequency of the ultrasonic probes [25]. Therefore, vibrational frequencies 20kHz, 24kHz and 28kHz were selected for this study and the calculation results of thermoelastic damping were $6.31e^{-6}$, $5.26e^{-6}$ and $4.50e^{-6}$, respectively.

Table 1
Material properties of AL7075-T6 [26]

Properties	Value
Density (kg/m^3)	2810
Young's modulus (GPa)	71.7
Poisson ratio	0.32
Thermal conductivity ($W/m°C$)	130
Specific heat ($J/Kg.°C$)	826.6
Thermal expansion ($1/°C$)	22.91

2.2 Finite Element Method in ANSYS

The FEM of two-dimensional model was developed in ANSYS to simulate the heat generation in the vibrating specimen. The specimen model had the dimension in length of 200 mm and thickness of 5 mm. The width of surface crack was 0.03 mm, crack depth was 3 mm and the remaining thickness at the crack location was 2 mm as shown in Figure 1. The specimen was AL7075-T6 and its properties were presented in Table 1. In ANSYS, the element type PLANE223 was used for the coupled structural-thermal analysis. The mesh size on crack location was 0.01 mm, while the mesh size on non-defect location was 0.5 mm. The mesh type was the triangular cell. Each cell had 6 nodes and each node had 3 degrees of freedom (displacement X, Y and temperature).

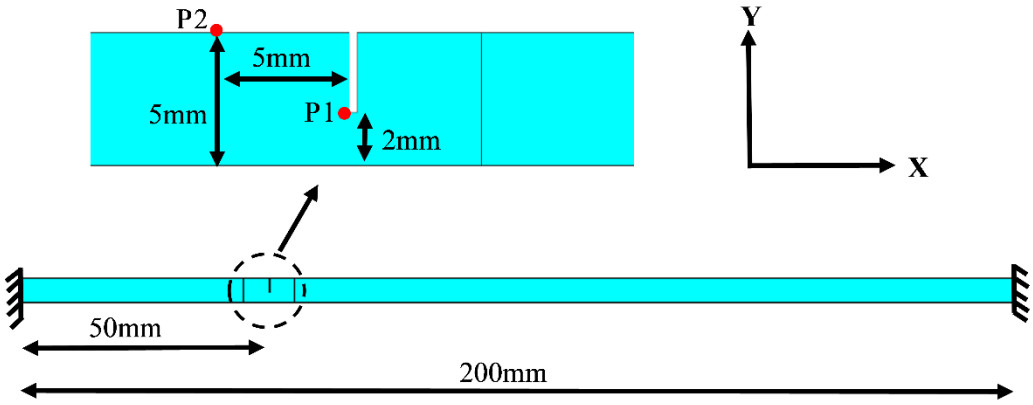

Fig. 1. Geometry model of specimen

Transient analysis was performed to simulate the dynamic response of stress and the heat generation on the vibrating specimen. The initial temperature of specimen was given at 27°C. On the left and right side ends of the specimen were fixed to zero displacement load (X, Y). While the surface crack area (P1) was applied with the sinusoidal displacement load which was assumed to have the maximum displacement load of 4.8 nm. In each case of simulation, the total vibrational period was 0.02 seconds and each cycle of vibration was decided to have 8 substeps.

3. Results and Discussions

The simulation results of the case study with 20kHz are used to represent the characteristic of temperature variation, stress variation and strain variation. The result of temperature variation at the crack location (P1) is shown in Figure 2. It can be seen that the characteristic of temperature variation can be divided into three periods A, B and C. For the period A, the initial heat generation increases the temperature up to 27.21°C and then gradually reduces. This is because the generated heat at the crack location flows to the surrounding area where has the lower temperature. This

explanation is proved by the graphical results of the temperature distribution and the flux vector in Figure 3. For the case study with the vibrational frequency 24kHz and 28kHz also have the same characteristic of temperature variation during period A. The maximum increment of temperature at the initial vibration of these two frequencies are 27.21°C and 27.26°C, respectively. For the vibrational period B, the temperature variation tends to be constant and slowly increases in the vibrational period C. It indicates that the response of heat generation and temperature increment at crack location is very fast and less than 1 second. The average of the temperature difference between crack location (P1) and non-defect location (P2) is determined during period B and C. The average of temperature difference of these three cases are 0.02°C as shown in Table 2. The thermal imaging camera such as IRCAM EQUUS 327 has the temperature sensitivity up to 0.02 °C which is able to capture the temperature difference for these case studies [27]. However, the case study with the higher temperature difference is easier to identify the defect location.

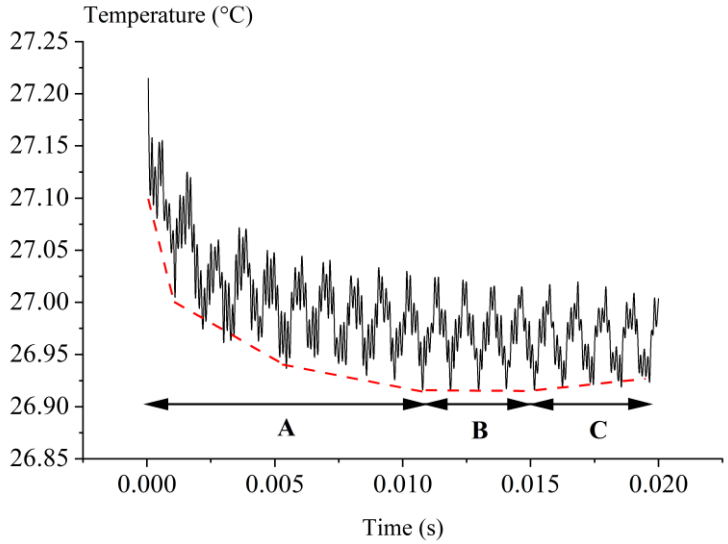

Fig. 2. Temperature variation at crack location (P1) of case study 20kHz

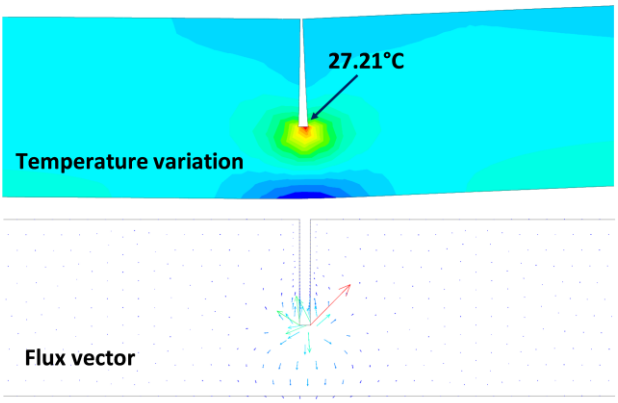

Fig. 3. Temperature variation and heat flow direction at crack location (P1) of case study 20kHz

The stress variation at the crack location is analyzed to confirm that the plastic deformation does not occur in this study. Because the deformation of the specimen in the plastic range is permanent which is not the concept of the non-destructive testing (NDT). The maximum stress of case studies with 20kHz, 24kHz and 28kHz occur at the crack location and have the maximum value of 140 MPa, 151 MPa and 195 MPa, respectively. All case studies have the maximum stress less than the yield stress of AL7075-T6 which is 503 MPa [28]. Therefore, plastic deformation does not have any effect on vibrothermography under these conditions. When consider the influence of the vibrational frequency over the stress, the case study with the higher frequency tends to produce the higher stress. Even though all case studies are controlled to have the same maximum vibrational amplitude. Figure 4 and Figure 5 are presented the results of temperature and stress variation in the different time frame of case study 20kHz. During time frame 0.005s, 0.010s and 0.020s are compression cycle and high temperature is produced at crack location. While the time frame 0.015s is expansion cycle and the high temperature is produced on the opposite side with the crack location. It can be seen that the high stress concentration occurs at the crack location either compression or expansion cycle. Therefore, the temperature at the crack location is always higher than non-defect location.

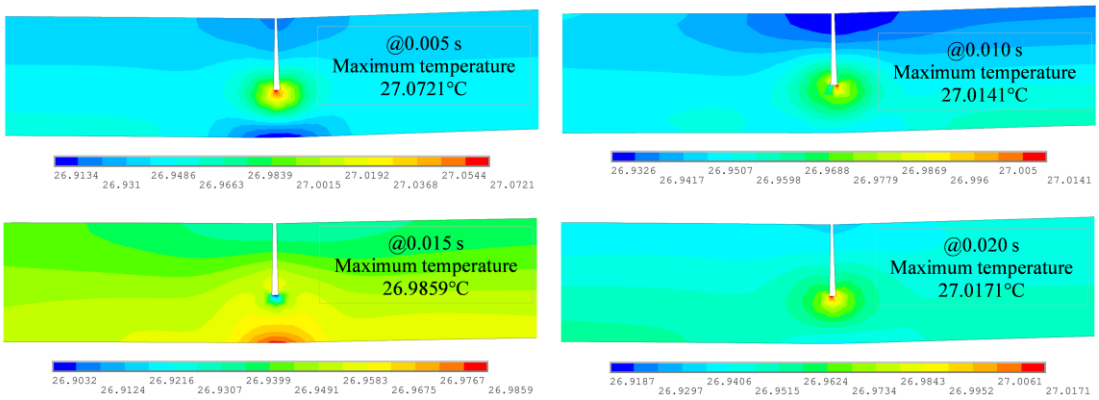

Fig. 4. Temperature variation at different time frames of case study 20kHz

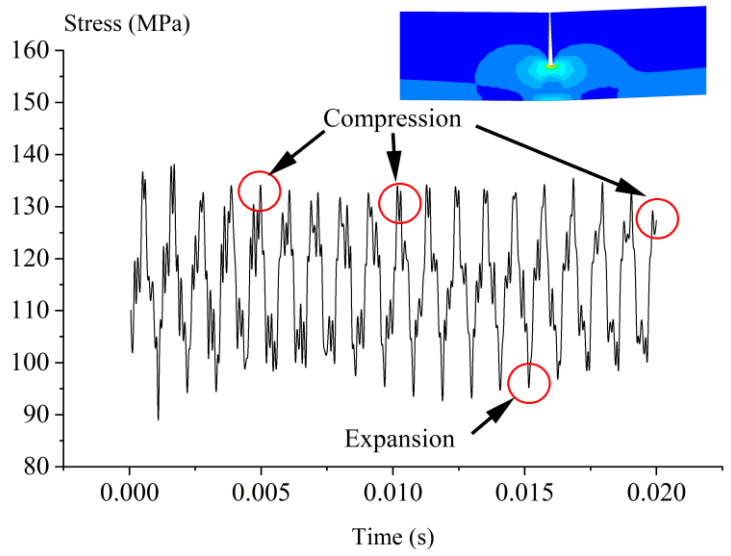

Fig. 5. Stress variation at crack location (P1) of case study 20kHz

The simulation results of strain energy are used to represent the input energy. For the case study with 20kHz, the result of strain energy at the crack location (P1) is presented in Figure 6. The maximum strain energy is obtained during the compression cycle, while the minimum strain is obtained during the expansion cycle. In each time step, the strain energy is multiplied with the thermoelastic damping (Q^{-1}) to obtain the mechanical energy loss (E_L) as heat. To obtain the power loss, the total energy loss during the vibrational period 0.02s is summed and calculated for 1s. The results of power loss (P_L) of case studies 20kHz, 24kHz and 28kHz are $8.71e^{-5}$, $8.72e^{-5}$ and $8.73e^{-5}$ J/s which is less significant different between these three case studies as shown in the Table 2.

The mean value of heat flow rate from crack location (P1) is considered during the vibrational period B and C, because the temperature variation during these periods are more stable than the initial vibration of period A. The results of heat flow rate (H_F) of frequencies 20kHz, 24kHz and 28kHz are 2.48 J/s, 2.65 J/s and 2.74 J/s, respectively. It can be seen that the heat flow rate increases with increasing of the vibrational frequency. The ratio between the mechanical power loss (P_L) and the heat flow rate (H_F) is determined to predict the suitable vibrational frequency that tends to have a high accumulation of heat at the crack location. The results of the index ratio for 20kHz, 24kHz and 28kHz are $3.50e^{-5}$, $3.28e^{-5}$ and $3.18e^{-5}$, respectively. The index ratio of case study 20kHz is higher than case studies 24kHz and 28kHz at 6.29% and 9.14% respectively. Therefore, frequency 20kHz is the more suitable for using as the vibrational frequency of these case studies.

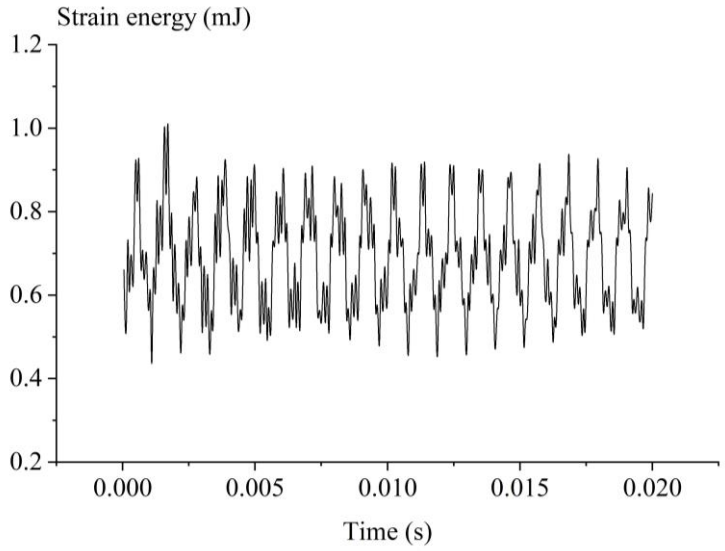

Fig. 6. Strain energy variation at crack location (P1)

Table 2
Simulation results

Frequency	Maximum Temperature at P1	ΔT: P1vs P2 Time 0.01-0.02	(Q^{-1})	Power loss (P_L)	Mean value of heat flow (H_F)	Ratio P_L/H_F
20 kHz	27.21°C	0.02°C	$6.31e^{-6}$	$8.71e^{-5}$ J/s	2.4884 J/s	$3.50e^{-5}$
24 kHz	27.21°C	0.02°C	$5.26e^{-6}$	$8.72e^{-5}$ J/s	2.6564 J/s	$3.28e^{-5}$
28 kHz	27.26°C	0.02°C	$4.50e^{-6}$	$8.73e^{-5}$ J/s	2.7444 J/s	$3.18e^{-5}$

4. Conclusions

The FEM model of vibrating specimen was successful to simulate the heat generation on crack location based on the effect of thermoelastic damping. The simulation was performed with constant vibrational amplitude at 4.8nm and varied the vibrational frequency at 20kHz, 24kHz and 28kHz. The simulation results indicated that the generated heat was high enough to make the temperature difference between crack location and non-defect location. For the vibrational period 0.02s, all case studies had the temperature difference between crack and non-defect locations around 0.02°C which was in the range of thermal imaging camera such as IRCAM EQUUS 327. The amount of the generated heat depended directly with the stress concentration on the specimen. This statement was true because the crack location was weak and the vibrational amplitude was higher than the surrounding area. Then the high stress concentration occurred on the crack surface during the compression cycle and resulted of the high temperature on crack surface. While the expansion cycle, the high stress concentration and temperature appeared on the opposite surface of the crack. Moreover, the effect of using high vibrational frequency produced the higher stress as comparing with the case study of low frequency. The lower stress implied the lower of fatigue problems. Therefore, a case study with lower vibration will be a better solution if the results the temperature variation between cases of high and low frequency was not different. The power loss of each case study was calculated and the results were less significant difference between these three cases. The power loss of cases 20kHz, 24kHz and 28kHz were $8.71e^{-5}$, $8.72e^{-5}$ and $8.73e^{-5}$, respectively. For the heat flow rate, it was measured at crack location and it tended to increase with increasing of vibrational frequency. Finally, the ratio between power loss and the heat flow rate was used to determine the case study with a high accumulation of heat at crack location. The result of the index ratio of case study 20kHz was higher than case studies with 24kHz, 28kHz at 6.29% and 9.14%, respectively. Therefore, the vibrational frequency 20kHz can be considered as the most suitable vibrational frequency because this frequency tended to have lower fatigue problems and high accumulation of heat as referring to the stress result and the ratio between power loss and heat flow rate.

Acknowledgement
This research was not funded by any grant.

References
[1] Favro, L. D., R. L. Thomas, Xiaoyan Han, Zhong Ouyang, Golam Newaz, and Dominico Gentile. "Sonic infrared imaging of fatigue cracks." *International journal of fatigue* 23 (2001): 471-476. https://doi.org/10.1016/S0142-1123(01)00151-7

[2] Holland, Stephen D., Christopher Uhl, Zhong Ouyang, Tom Bantel, Ming Li, William Q. Meeker, John Lively, Lisa Brasche, and David Eisenmann. "Quantifying the vibrothermographic effect." *NDT & E International* 44, no. 8 (2011): 775-782. https://doi.org/10.1016/j.ndteint.2011.07.006

[3] Fierro, Gian Piero Malfense, Dmitri Ginzburg, Francesco Ciampa, and Michele Meo. "Nonlinear ultrasonic stimulated thermography for damage assessment in isotropic fatigued structures." *Journal of Sound and Vibration* 404 (2017): 102-115. https://doi.org/10.1016/j.jsv.2017.05.041

[4] Plum, Robin, and Thomas Ummenhofer. "Structural-thermal finite element simulation of vibrothermography applied to cracked steel plates." *Quantitative InfraRed Thermography Journal* 8, no. 2 (2011): 201-220. https://doi.org/10.3166/qirt.8.201-220

[5] Ibarra-Castanedo, Clemente, Jean-Marc Piau, Stéphane Guilbert, Nicolas P. Avdelidis, Marc Genest, Abdelhakim Bendada, and Xavier PV Maldague. "Comparative study of active thermography techniques for the nondestructive evaluation of honeycomb structures." *Research in Nondestructive Evaluation* 20, no. 1 (2009): 1-31. https://doi.org/10.1080/09349840802366617

[6] Hedayatrasa, Saeid, Joost Segers, Gaétan Poelman, Wim Van Paepegem, and Mathias Kersemans. "Sweep vibrothermography and thermal response derivative spectroscopy for identification of local defect resonance

frequencies of impacted CFRP." In *Proceedings of Meetings on Acoustics*, vol. 38, no. 1. AIP Publishing, 2019. https://doi.org/10.1121/2.0001063

[7] Hettler, Jan, Morteza Tabatabaeipour, Steven Delrue, and Koen Van Den Abeele. "Detection and characterization of local defect resonances arising from delaminations and flat bottom holes." *Journal of Nondestructive Evaluation* 36, no. 1 (2017): 2. https://doi.org/10.1007/s10921-016-0380-6

[8] Mukhtar, A., M. A. Khattak, I. S. Shahid, and M. S. M. Sufian. "A review on application of non destructive techniques on composites." *Journal of Advanced Research in Applied Mechanics* 20, no. 1 (2016): 12-21.

[9] Renshaw, Jeremy, John C. Chen, Stephen D. Holland, and R. Bruce Thompson. "The sources of heat generation in vibrothermography." *Ndt & E International* 44, no. 8 (2011): 736-739. https://doi.org/10.1016/j.ndteint.2011.07.012

[10] Bhargava, Vibhor, Bassam A. Abu-Nabah, and Maen Alkhader. "A theoretical approach towards the modeling of vibrothermography using finite element methods." *European Journal of Mechanics-A/Solids* 91 (2022): 104389. https://doi.org/10.1016/j.euromechsol.2021.104389

[11] Dong, Lihong, Bozheng Wang, Haidou Wang, Ming Xiang, Xi Chen, Guozheng Ma, Yuelan Di, Wei Guo, Jiajie Kang, and Xinyuan Zhou. "Effects of crack surface roughness on crack heat generation characteristics of ultrasonic infrared thermography." *Infrared Physics & Technology* 106 (2020): 103262. https://doi.org/10.1016/j.infrared.2020.103262

[12] Mabrouki, Farid, Marc Thomas, M. Genest, and A. Fahr. "Frictional heating model for efficient use of vibrothermography." *NDT & E International* 42, no. 5 (2009): 345-352. https://doi.org/10.1016/j.ndteint.2009.01.012

[13] Rosakis, P., A. J. Rosakis, G. Ravichandran, and J. Hodowany. "A thermodynamic internal variable model for the partition of plastic work into heat and stored energy in metals." *Journal of the Mechanics and Physics of Solids* 48, no. 3 (2000): 581-607. https://doi.org/10.1016/S0022-5096(99)00048-4

[14] Mabrouki, Farid, Marc Thomas, M. Genest, and A. Fahr. "Numerical modeling of vibrothermography based on plastic deformation." *NDT & E International* 43, no. 6 (2010): 476-483. https://doi.org/10.1016/j.ndteint.2010.05.002

[15] Vaddi, Jyani S., Stephen D. Holland, and Michael R. Kessler. "Absorptive viscoelastic coatings for full field vibration coverage measurement in vibrothermography." *NDT & E International* 82 (2016): 56-61. https://doi.org/10.1016/j.ndteint.2016.04.004

[16] Kostina, Anastasiia, Oleg Plekhov, and Sergey Aizikovich. "Numerical simulation of a heat generation in a layered material during ultrasonic wave propagation." *Frattura ed Integrità Strutturale* 12, no. 46 (2018): 332-342. https://doi.org/10.3221/IGF-ESIS.46.30

[17] Guo, Xingwang, and Liang Zhu. "Vibro-thermography of calibrated defects in hybrid plates focusing on viscoelastic heat generation." *Quantitative InfraRed Thermography Journal* 18, no. 5 (2021): 314-331. https://doi.org/10.1080/17686733.2020.1771528

[18] Rizi, A. Saboktakin, S. Hedayatrasa, X. Maldague, and Toan Vukhanh. "FEM modeling of ultrasonic vibrothermography of a damaged plate and qualitative study of heating mechanisms." *Infrared Physics & Technology* 61 (2013): 101-110. https://doi.org/10.1016/j.infrared.2013.07.011

[19] Blanter, Mikhail S., Igor S. Golovin, H. Neuhauser, and Hans-Rainer Sinning. *Internal friction in metallic materials*. Berlin: Springer, 2007. https://doi.org/10.1007/978-3-540-68758-0

[20] Lifshitz, Ron, and Michael L. Roukes. "Thermoelastic damping in micro-and nanomechanical systems." *Physical review B* 61, no. 8 (2000): 5600. https://doi.org/10.1103/PhysRevB.61.5600

[21] Sun, Yuxin, Daining Fang, and Ai Kah Soh. "Thermoelastic damping in micro-beam resonators." *International Journal of Solids and Structures* 43, no. 10 (2006): 3213-3229. https://doi.org/10.1016/j.ijsolstr.2005.08.011

[22] Hodonou, C., Marek Balazinski, Myriam Brochu, and Christian Mascle. "Material-design-process selection methodology for aircraft structural components: application to additive vs subtractive manufacturing processes." *The International Journal of Advanced Manufacturing Technology* 103 (2019): 1509-1517. https://doi.org/10.1007/s00170-019-03613-5

[23] Aamir, Muhammad, Khaled Giasin, Majid Tolouei-Rad, and Ana Vafadar. "A review: Drilling performance and hole quality of aluminium alloys for aerospace applications." *Journal of Materials Research and Technology* 9, no. 6 (2020): 12484-12500. https://doi.org/10.1016/j.jmrt.2020.09.003

[24] Abd El-Hameed, Afaf M., and Y. A. Abdel-Aziz. "Aluminium Alloys in Space Applications: A Short Report." *Journal of Advanced Research in Applied Sciences and Engineering Technology* 22, no. 1 (2021): 1-7. https://doi.org/10.37934/araset.22.1.17

[25] Ngaongam, Choosak, Mongkol Ekpanyapong, and Rapee Ujjin. "Surface crack detection by using vibrothermography technique." *Quantitative InfraRed Thermography Journal* (2022): 1-12. https://doi.org/10.1080/17686733.2022.2121102

[26] Lee, Hwa-Teng, and G. H. Shaue. "The thermomechanical behavior for aluminum alloy under uniaxial tensile loading." *Materials Science and Engineering: A* 268, no. 1-2 (1999): 154-164. https://doi.org/10.1016/S0921-5093(99)00069-6

[27] Solodov, Igor, Markus Rahammer, Daria Derusova, and Gerd Busse. "Highly-efficient and noncontact vibro-thermography via local defect resonance." *Quantitative InfraRed Thermography Journal* 12, no. 1 (2015): 98-111. https://doi.org/10.1080/17686733.2015.1026018

[28] Zhou, Guo Wei, Da Yong Li, and Ying Hong Peng. "Investigation of tensile deformation behavior of 7075-T6 at elevated temperatures." *Applied Mechanics and Materials* 152 (2012): 358-363. https://doi.org/10.4028/www.scientific.net/AMM.152-154.358